ADVANCED FUNCTIONAL MATERIALS
www.afm-journal.de

Plasmonic Color Filters as Dual-State Nanopixels for High-Density Microimage Encoding

*Esmaeil Heydari, Justin R. Sperling, Steven L. Neale, and Alasdair W. Clark**

Plasmonic color filtering has provided a range of new techniques for "printing" images at resolutions beyond the diffraction-limit, significantly improving upon what can be achieved using traditional, dye-based filtering methods. Here, a new approach to high-density data encoding is demonstrated using full color, dual-state plasmonic nanopixels, doubling the amount of information that can be stored in a unit-area. This technique is used to encode two data sets into a single set of pixels for the first time, generating vivid, near-full sRGB (standard Red Green Blue color space)color images and codes with polarization-switchable information states. Using a standard optical microscope, the smallest "unit" that can be read relates to 2 × 2 nanopixels (370 nm × 370 nm). As a result, dual-state nanopixels may prove significant for long-term, high-resolution optical image encoding, and counterfeit-prevention measures.

1. Introduction

The ability to effectively separate discrete colors from white light lies at the heart of how we record and view optical information, whether that be the arrangement of colored inks in painting and printing applications, or the spectral filters that enable many modern image display and recording technologies. In each case, color separation is typically provided by organic compounds, dyes, and pigments that absorb and scatter particular wavelengths of light, leading to their distinct color profiles. Recently, structural color systems based on engineered nanophotonic materials have emerged as an appealing alternative to absorptive dyes.[1–12] Among these examples are color filters based on plasmonics; filters which rely on the resonant interaction between incident photons and the free-electrons of nanoscale metal structures. Thus far, filters based on positive nanostructures,[4,7,9,11–15] filters based on cavity apertures,[2,16–18] and filters which combine both strategies[8] have been shown, each with distinct fabrication and geometrical solutions to achieving color "nanopixels" for selective white-light separation. Plasmonic pixels, in their various forms, hold several advantages over their microscale, dye-based counterparts. Chief among these are their subwavelength dimensions (leading to ultradense, ultrathin pixel arrays), and their long-term environmental stability (they do not degrade or fade over time due to radiation exposure). As a result, plasmonic filters have been positioned as new technological solutions for subwavelength color printing,[1,4,7–9,12] anticounterfeiting measures,[19,20] and RGB splitting for image sensors;[2,17,21,22] thus representing one of the most promising, technologically relevant areas of current plasmonic research activity. Here, we explore a new application of polarization-controlled plasmonic filters: dual output, full-color optical image encoding.

Recent developments in the engineering and manipulation of materials on the nanoscale have given rise to a number of new techniques with the potential for physically encoding data and images into optically readable volumes and surfaces.[23,24] Using semiconductor quantum dots,[25–27] graphene,[28] and various super-resolution lithography techniques,[29–34] researchers are demonstrating novel 2D and 3D techniques that may enable the next generation of optical storage and encoding technologies. Plasmonic particles and filters have also seen applications in these research areas, with the aforementioned image encoding examples having been joined by demonstrations of their use in optical data storage.[23,24,35–37] Here, we show a new utilization of image encoding using polarization multiplexed plasmonic filters, where, unlike previous studies that employed color or position switching in fixed images,[14,38] we show that two arbitrary, full-color images can be encoded into a single array of pixels. Our individual pixels are comprised of asymmetric cross-shaped nanoapertures in a thin film of aluminum. Each aperture is engineered to exhibit two independent plasmonic resonances which can be tuned across the sRGB (standard Red Green Blue) color-space (a single pixel can be encoded with any two arbitrary colors). We go on to show that by using the smallest visible unit of these apertures (2 × 2 apertures, measuring ≈370 nm × 370 nm) as high-resolution coding-elements we can create high-density QR codes that contain two optically-readable outputs.

2. Results and Discussion

The color pixels were constructed as cross-shaped apertures in a 100 nm aluminum film deposited on a borosilicate substrate and capped with a 150 nm layer of SiO_2 (using a combination of metal-evaporation, electron-beam lithography,

Dr. E. Heydari, J. R. Sperling, Dr. S. L. Neale,
Prof. A. W. Clark
Biomedical Engineering Research Division
School of Engineering
University of Glasgow
Glasgow G12 8LT, UK
E-mail: alasdair.clark@glasgow.ac.uk

DOI: 10.1002/adfm.201701866

reactive ion etching, and inductively coupled plasma deposition). Al was chosen as our plasmonic material due to its wide spectral plasmonic band, which can be tuned from the UV to the NIR, its low-cost, and its compatibility with current semiconductor manufacturing processes. Acting as a filter for white light, the color response of the individual pixels was tuned by altering the arm-length and periodicity of the cross structures. The cross-structure itself enables polarization dependence due to the selection rules for light propagation through a nanoscale slit, which requires the electric-field component of the incident light to be perpendicular to the length of the slit (**Figure 1**a). As a result, the two perpendicular arm sections of the cross can support their own resonance properties that can be tuned independently of one another, with zero color-leaking between modes.

Figure 1b shows a polarization-switchable color palette made using these structures. The palette is comprised of 21 × 21 pixel arrays, each with different design parameters. By independently varying the "arm-lengths" of the cross in each axis, as well as the period of the array in each axis, we can create a full range of visible colors at each polarization of white light. Moving from top to bottom, the length of the *x*-axis arm is increased from 120 to 220 nm, in 5 nm increments, (measured by SEM as 112 ± 5 nm to 219 ± 9 nm [SD]) while the period in the *y*-axis is decreased from 350 to 250 nm, in 5 nm increments. Moving from left to right, the length of the *y*-axis arm is decreased from 220 to 120 nm, while the period in the *x*-axis is increased from 250 to 350 nm. In all cases, the width of the arms is fixed at 20 nm (measured by SEM as 21 ± 2 nm [SD]). As a result, the top-left and bottom-right halves of the palette, as marked in Figure 1b, are the inverse of one another (i.e., the array in the upper-top-left of the palette is the same as the array in the lower-bottom-right, but rotated through 90°). The arrays which sit directly on the dividing line (Figure 1b) have identical dimensions and periods in *x* and *y*. As can be seen from Figure 1b, both the arm length (perpendicular to the electric-field) and periodicity (parallel to the electric-field) of the structures affect the pixel color; red-shifting as either value is increased. The periodicity of the pixels also dictates the sharpness of each resonance (the resonance becoming broader with decreasing interpixel distance) and the transmission efficiency (longer arms letting through a higher percentage of light). As a result, to achieve any one particular color there is a compromise between transmission percentage, spectral width, and peak position.

Using the previously stated dimensions, we can create a palette that encompasses the visible spectrum, running from deep blue to magenta. This palette by no means demonstrates all of the colors we can create, but instead the colors that can be accessed using the previously stated dimensional constraints. Choosing a minimum pixel period of 250 nm allows us to increase the arm-length of neighboring pixels to 220 nm without them merging. These constraints were not arbitrarily chosen, but instead translate to the widest color gamut available while maintaining the ability to encode both extremes of the color range into a single pixel geometry (outputting magenta in one polarization, blue in another). In other words, it is the best compromise that allows us to span the visible spectrum in both polarizations.

Figure 1c shows spectral analysis of 22 pixels arrays, selected from Figure 1b-i, that best represent the color range attainable using cross-shaped nanoapertures. Many of the pixel arrangements support both the high-frequency and the low-frequency resonance modes. For the majority of the palette, the high-frequency mode either occurs below 400 nm, or is so weak that its presence does not affect the perceived color output. As a result, increasing the arm-length or period results in a predictable "red-shift" of the spectra, and the perceived color output. However, for pixel arrays with larger transmission arm-lengths and periods, a strong mode can appear between 400 and 450 nm. This is the case for the magenta outputs. While the low-frequency "red" peak occurs between 650 and 700 nm for these pixels, the strong "blue" peak contributes to the perceived color, resulting in a mixture of the two, and producing magenta. By balancing these various spectral characteristics it would be possible to encode any single pixel with any two visible colors, giving us access to far too many variants than would be practical to demonstrate here. Figure 1d shows a CIE XY chromaticity diagram for the same 22 pixel array selection as Figure 1c, giving a clear representation of the color range accessible using these parametric constraints. The vibrancy and range of color that can be seen in Figure 1c are also seen here. The selected pixels show that we have coverage extending across the extremities of the majority of the sRGB color space (marked as a triangle on the diagram).

One of the major motivating factors driving the development of plasmonic color technology is the potential it holds for ultrahigh-resolution image "printing", with nanoscale pixel components facilitating print resolutions far beyond the diffraction limit.[9] By employing asymmetric pixels that can support polarization dependent resonances, further versatility is possible. Individual pixels that can encode two color profiles allow for images which have dual color states[38,39] and stereoscopic properties.[14] Here, we show that it is possible to use a single array of cross-shaped apertures to encode two full-color images into the same unit area, using the same set of nanopixels.

Figure 2 shows bright-field microscopy images of two distinct color patterns, each produced from the same pixel array. Through appropriate design and arrangement of the individual pixels, we have engineered a patterned white-light filter that, when illuminated from the rear, produces one of the two images, each linked to a different polarization (Figure 2a). As an example of the ability to produce dual, polarization-dependent information states in the same space, we have chosen to display microimages of the University of Glasgow crest when the light is polarized along the *y*-axis of the array, and the University's main building when the light is polarized along the *x*-axis of the array. The "arms" of each cross have been tuned to transmit the color appropriate to the desired image at each polarization. Since each aperture can produce any two visible colors, it is possible to encode any two arbitrary, full-color images or information sets into the same area using the same pixels (as can be seen from both Figures 1b and 2, there is no color leaking between polarizations).

Using dual-resonance pixels in this manner enables nanostructured surfaces to be produced which have double the information density of those which use single resonance pixels, a feature that could be used in long-term optical image storage applications. Nanophotonic solutions have recently emerged as an attractive addition to the field of information

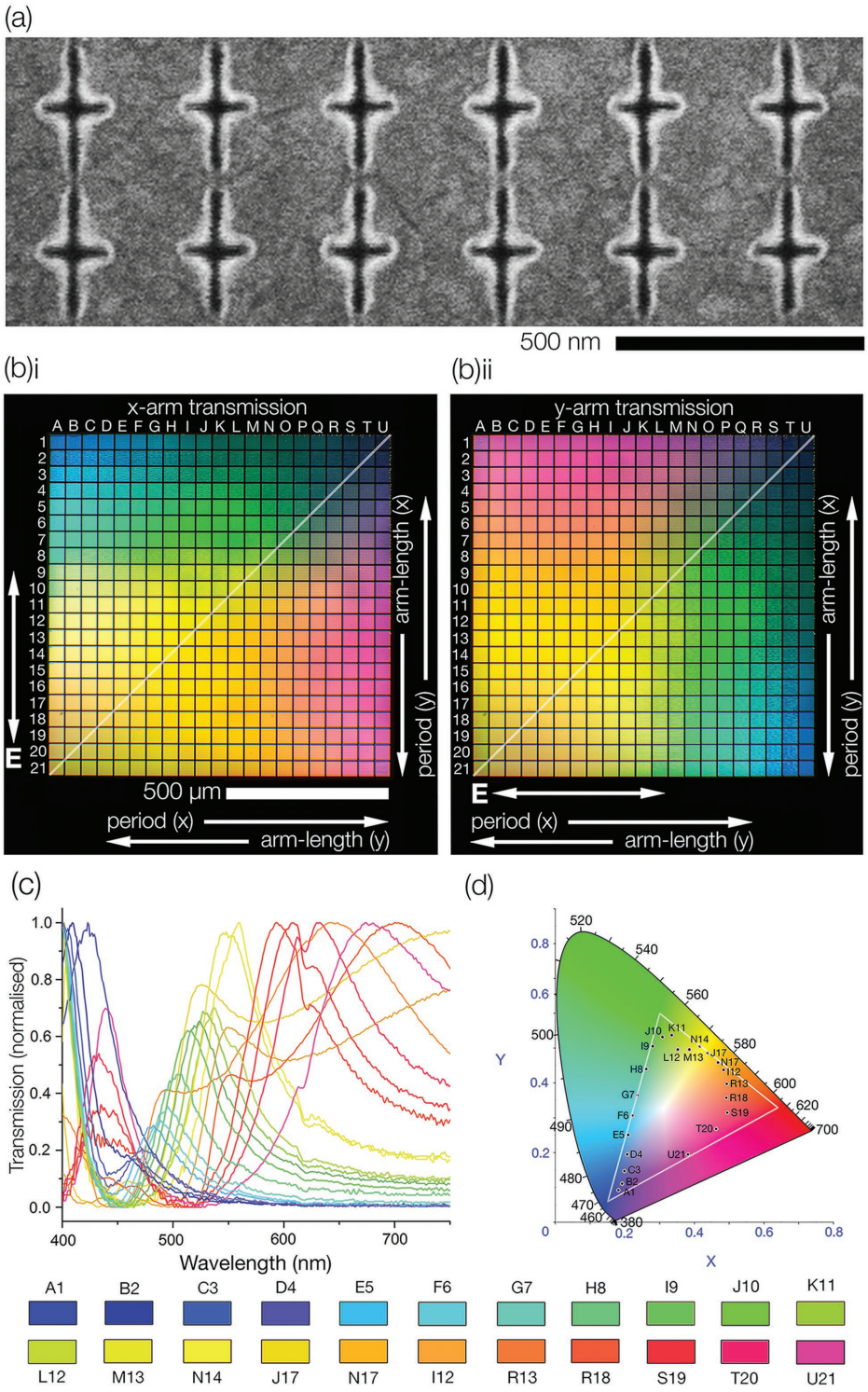

Figure 1. Nanopixel properties. a) SEM of a typical pixel array. SEM was taken before the deposition of the SiO_2 layer. b-i,ii) Bright-field microscope images showing a switchable color palette with different color outputs linked to different white-light polarizations. The geometry and period of each pixel array have been altered across the palette to produce a color range that spans the visible spectrum, and where both extremes of the range can be encoded into the same pixel (blue and magenta). The pixel arrays are labeled A1–U21. Moving from top to bottom the arm length in the *x*-axis is increased while the *y*-axis period is decreased. Moving from left to right the arm-length in the *y*-axis is decreased while the *x*-axis period is increased. The arm width is fixed. The pixel arrays on either side of the diagonal line are the inverse of one another (i.e., the *x*-axis period and arm-length of the array in the top-left of the palette have the same values as the *y*-axis period and arm-length of the array in the bottom-right). c) Normalized *x*-arm transmission spectra selected from the pixel arrays shown, and labeled, in (b-i), to best demonstrate the color range we can achieve across the visible spectrum. d) The same selection of pixel arrays plotted on a CIE XY chromaticity diagram. The sRGB color space is marked by the white triangle.

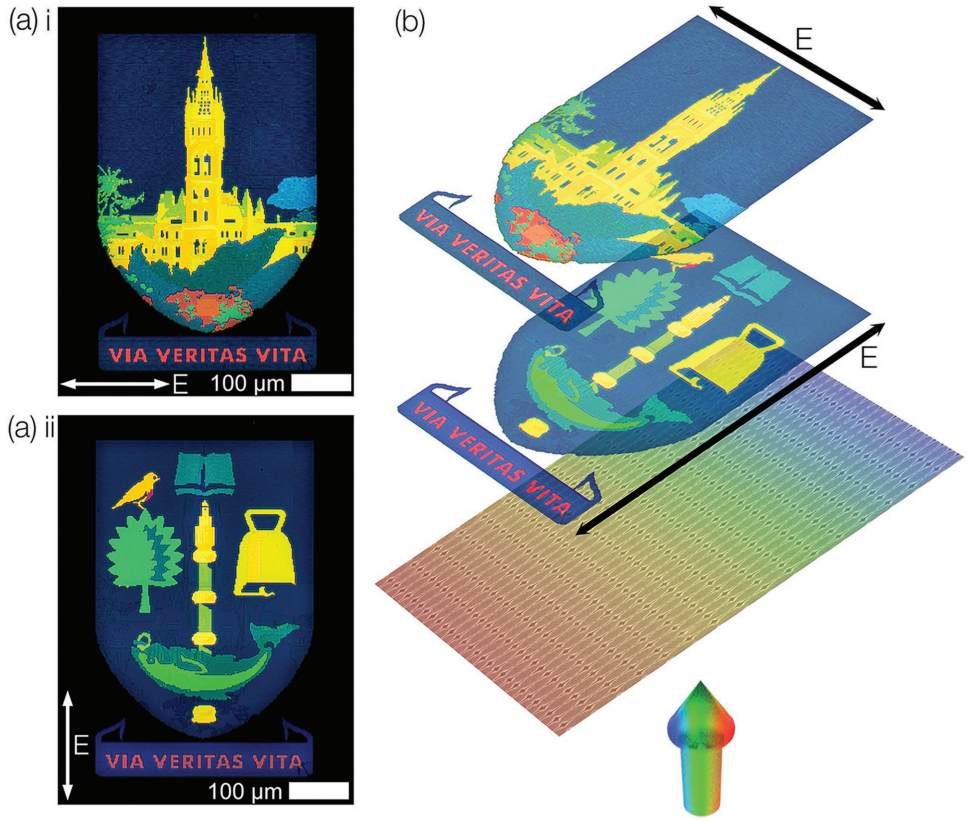

Figure 2. Bright-field microscope images showing the switchable nature of the information displayed by a single set of nanopixels. a) Bright-field transmission images showing the full-color pictures produced by the array when illuminated from the rear with white light at different polarizations. Switching the polarization of light causes the image displayed in the far-field to switch. b) Schematic showing how the images were taken. A white-light source passes through a linear polarizer before being selectively transmitted through the nanoapertures (pixels). At each polarization state the aperture transmits color corresponding to the desired display pattern.

storage and display,[23,35] as their employment allows for optically readable storage at the diffraction-limit that, unlike magnetic or electronic methods, can provide stable, long-term data retention in scenarios where heat, humidity, or radiation damage may be a concern. Having the scope to encode two color images at nanoscale resolutions into the same area may also make this technology appealing for the creation of anti-counterfeiting labels for bank-notes and high-value goods; labels that would be significantly more difficult to forge than current examples. Using a color-based pixel system allows for another advantage: the stored information, in this case micro-images, can be "read" using white light, a standard microscope, and the human eye.

The pixel density we can achieve using cross-shaped apertures varies with color due to the periodicity changes required to achieve a full color palette. As a result, we can achieve a density range that spans pixels-per-inch (PPI) values of 101 599 PPI at its most dense, and 72 568 PPI at its most sparse. These values represent the number of physical apertures in a single inch, in any one axis (the periods in *X* and *Y* may differ depending on the desired 2-color pixel response). Since we can encode both "arms" of any one aperture with its own color profile, we are able to effectively double this PPI range in terms of useful image encoding density. However, in order to determine the ultimate usable capacity of this system, we must determine the size limit below which individual groups of pixels cannot be resolved using white light.

Figure 3 shows an ultrahigh-density QR code encoded with two layers of information. These QR codes have feature sizes beyond the diffraction limit that are nevertheless visible using a simple optical microscope. QR codes are comprised of a matrix of contrasting modules, the layout of which defines a 2D barcode. After fabricating a range of codes using different pixel numbers per module, it was determined that the smallest color feature that can be resolved using white light and a standard optical microscope comprises 2 × 2 nanopixels (at a period of 250 nm). The dual-state code in Figure 3 has outputs relating to the homepage URLs of Advanced Functional Materials and the University of Glasgow's School of Engineering. The 16 μm × 16 μm codes (the smallest possible using the 2 × 2 pixel per QR-module limit) are clearly visible using a 100× objective lens, and both information outputs can be easily decoded using a mobile phone QR-reader application. At this level, color separation from immediately adjacent pixel groupings is maintained, as is the polarization switching capability (green boxes marked in Figure 3a-i,ii. This visible-pixel density relates to an area of 370 nm × 370 nm for the smallest features we demonstrate here (period + arm-length). We believe these to be the smallest, most information dense, optically resolvable QR codes demonstrated to date.

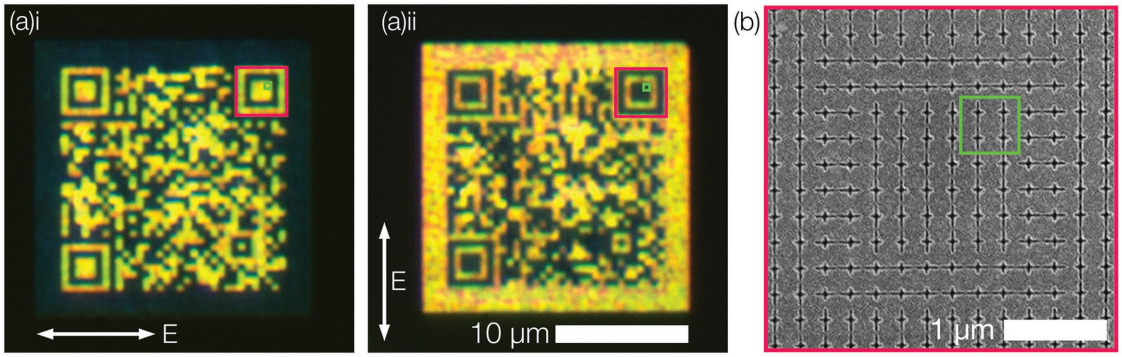

Figure 3. Bright-field and SEM images of a switchable QR-code. a-i,ii) Bright-field images of a 16 µm QR code (20 µm with border included) taken using a 100× objective lens when the illuminating white light is polarized along the *x* and *y* axes of the code, respectively. A different QR code is visible at each polarization state. To view the information stored within the dual-state QR code, a QR reader capable of scanning reversed contrast codes, such as I-nigma, is necessary (bright patterns on dark backgrounds). b) A wide-area SEM image showing the pattern present in the top-right corner of the QR code. SEM was taken before the deposition of the SiO_2 layer.

3. Conclusion

As the field of plasmonic color generation advances, there is a tremendous scope for devices based on these principles to be one of the few nanoplasmonic technologies that make the jump from research curiosity to commercial deployment. We have demonstrated a means of using dual-color nanopixels to encode two full-color information sets, whether they are images or codes, into the same unit area. As a result, this technology is positioned as a promising candidate for microimage encoding, particularly if the design principles were transferred to nanoimprinting technologies. Furthermore, with a PPI value exceeding 100 000, each able to encode two color states, this technology may also prove useful for high-resolution printing applications and counterfeit-prevention measures.

4. Experimental Section

Fabrication: The pixels were fabricated using a combination of metal-evaporation, electron-beam lithography, reactive ion etching, and inductively coupled plasma deposition. 100 nm of Al was deposited onto a 500 µm borosilicate substrate via electron-beam evaporation. The ZEP520A etch mask was patterned using a Vistec VB6 UHR EWF electron beam lithography tool. The cavity-apertures that comprised the individual pixels were then created using SiCl4 gas in an Oxford Instrument System 100 reactive ion etch tool. A 150 nm SiO_2 cap layer (added to enhance transmission) was deposited onto the etched Al film using an Oxford Instrument System 100 plasma deposition tool.

Optical Characterization: Bright-field images of the pixel arrays were captured using a Zeiss Axio Imager A1 optical microscope in conjunction with a Sony NEX-F3 camera. The Zeiss Epiplan-Neofluar objective lenses used included a 20 × 0.5 NA, a 50 × 0.5 NA, and a 100 × 0.75 NA. Plasmonic spectra were collected over the visible spectrum (400–700 nm) using a Shimadzu UV3101PC spectrophotometer and a linear film polarizer.

Data: All data relating to the work outlined in the article can be found at: http://dx.doi.org/10.5525/gla.researchdata.379.

Acknowledgements

E.H. and J.R.S. contributed equally to this work. The work was supported by the Royal Academy of Engineering (Grant No. 10216/103) and the EPSRC (Grant Nos. EP/P51133X/1 and EP/N016874/1). The authors also wish to thank all the staff working in the James Watt Nanofabrication Centre for their support.

Conflict of Interest

The authors declare no conflict of interest.

Keywords

color printing, image encoding, metasurfaces, nanopixels, plasmonic color filters

Received: April 7, 2017
Revised: June 2, 2017
Published online: July 31, 2017

[1] Y. Gu, L. Zhang, J. K. W. Yang, S. P. Yeo, C.-W. Qiu, *Nanoscale* **2015**, *7*, 6409.
[2] S. P. Burgos, S. Yokogawa, H. A. Atwater, *ACS Nano* **2013**, *7*, 10038.
[3] N. Dean, *Nat. Nanotechnol.* **2015**, *10*, 15.
[4] M. Miyata, H. Hatada, J. Takahara, *Nano Lett.* **2016**, *16*, 3166.
[5] A. W. Clark, J. M. Cooper, *Angew. Chem., Int. Ed.* **2012**, *51*, 3562.
[6] S. Yokogawa, S. P. Burgos, H. A. Atwater, *Nano Lett.* **2012**, *12*, 4349.
[7] S. J. Tan, L. Zhang, D. Zhu, X. M. Goh, Y. M. Wang, K. Kumar, C.-W. Qiu, J. K. W. Yang, *Nano Lett.* **2014**, *14*, 4023.
[8] T. D. James, P. Mulvaney, A. Roberts, *Nano Lett.* **2016**, *16*, 3817.
[9] K. Kumar, H. Duan, R. S. Hegde, S. C. W. Koh, J. N. Wei, J. K. W. Yang, *Nat. Nanotechnol.* **2012**, *7*, 557.
[10] F. Cheng, J. Gao, T. S. Luk, X. D. Yang, *Sci. Rep.* **2015**, *5*, 11045.
[11] A. S. Roberts, A. Pors, O. Albrektsen, S. I. Bozhevolnyi, *Nano Lett.* **2014**, *14*, 783.
[12] J. Olson, A. Manjavacas, L. Liu, W.-S. Chang, B. Foerster, N. S. King, M. W. Knight, P. Nordlander, N. J. Halas, S. Link, *Proc. Natl. Acad. Sci. USA* **2014**, *111*, 14348.
[13] T. H. Chen, B. M. Reinhard, *Adv. Mater.* **2016**, *28*, 3522.
[14] X. M. Goh, Y. Zheng, S. J. Tan, L. Zhang, K. Kumar, C.-W. Qiu, J. K. W. Yang, *Nat. Commun.* **2014**, *5*, 5361.
[15] Y. W. Huang, W. T. Chen, W. Y. Tsai, P. C. Wu, C. M. Wang, G. Sun, D. P. Tsai, *Nano Lett.* **2015**, *15*, 3122.

[16] V. R. Shrestha, S.-S. Lee, E.-S. Kim, D.-Y. Choi, *Nano Lett.* **2014**, *14*, 6672.
[17] B. Y. Zheng, Y. M. Wang, P. Nordlander, N. J. Halas, *Adv. Mater.* **2014**, *26*, 6318.
[18] R. Rajasekharan, E. Balaur, A. Minovich, S. Collins, T. D. James, A. Djalalian-Assl, K. Ganesan, S. Tomljenovic-Hanic, S. Kandasamy, E. Skafidas, D. N. Neshev, P. Mulvaney, A. Roberts, S. Prawer, *Sci. Rep.* **2014**, *4*, 6435.
[19] A. F. Smith, P. Patton, S. E. Skrabalak, *Adv. Funct. Mater.* **2016**, *26*, 1315.
[20] Y. H. Zheng, C. Jiang, S. H. Ng, Y. Lu, F. Han, U. Bach, J. J. Gooding, *Adv. Mater.* **2016**, *28*, 2330.
[21] Q. Chen, D. Das, D. Chitnis, K. Walls, T. D. Drysdale, S. Collins, D. R. S. Cumming, *Plasmonics* **2012**, *7*, 695.
[22] L. Frey, P. Parrein, J. Raby, C. Pellé, D. Hérault, M. Marty, J. Michailos, *Opt. Express* **2011**, *19*, 13073.
[23] M. Gu, X. P. Li, Y. Y. Cao, *Light: Sci. Appl.* **2014**, *3*, e177.
[24] M. Gu, Q. Zhang, S. Lamon, *Nat. Rev. Mater.* **2016**, *1*, 16070.
[25] J. W. M. Chon, P. Zijlstra, M. Gu, J. van Embden, P. Mulvaney, *Appl. Phys. Lett.* **2004**, *85*, 5514.
[26] J. Kimura, S. Maenosono, Y. Yamaguchi, *Nanotechnology* **2003**, *14*, 69.
[27] X. P. Li, J. W. M. Chon, R. A. Evans, M. Gu, *Opt. Express* **2009**, *17*, 2954.
[28] X. P. Li, Q. M. Zhang, X. Chen, M. Gu, *Sci. Rep.* **2013**, *3*, 4.
[29] L. Li, R. R. Gattass, E. Gershgoren, H. Hwang, J. T. Fourkas, *Science* **2009**, *324*, 910.
[30] Z. Gan, Y. Cao, R. A. Evans, M. Gu, *Nat. Commun.* **2013**, *4*, 2061.
[31] B. H. Cumpston, S. P. Ananthavel, S. Barlow, D. L. Dyer, J. E. Ehrlich, L. L. Erskine, A. A. Heikal, S. M. Kuebler, I. Y. S. Lee, D. McCord-Maughon, J. Q. Qin, H. Rockel, M. Rumi, X. L. Wu, S. R. Marder, J. W. Perry, *Nature* **1999**, *398*, 51.
[32] T. L. Andrew, H.-Y. Tsai, R. Menon, *Science* **2009**, *324*, 917.
[33] B. Harke, W. Dallari, G. Grancini, D. Fazzi, F. Brandi, A. Petrozza, A. Diaspro, *Adv. Mater.* **2013**, *25*, 904.
[34] M. P. Stocker, L. Li, R. R. Gattass, J. T. Fourkas, *Nat. Chem.* **2011**, *3*, 223.
[35] P. Zijlstra, J. W. M. Chon, M. Gu, *Nature* **2009**, *459*, 410.
[36] H. Ditlbacher, J. R. Krenn, B. Lamprecht, A. Leitner, F. R. Aussenegg, *Opt. Lett.* **2000**, *25*, 563.
[37] H. R. Ren, X. P. Li, Q. M. Zhang, M. Gu, *Science* **2016**, *352*, 805.
[38] Z. B. Li, A. W. Clark, J. M. Cooper, *ACS Nano* **2016**, *10*, 492.
[39] T. Ellenbogen, K. Seo, K. B. Crozier, *Nano Lett.* **2012**, *12*, 1026.